Heliyon 9 (2023) e23104

Contents lists available at ScienceDirect

Heliyon

journal homepage: www.cell.com/heliyon

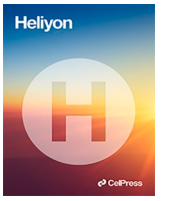

Effect of benzotriazole on the existing pits of copper tube in fire sprinkler system

Eun-Ha Park, Sang-Jin Ko, Jung-Gu Kim *

School of Advanced Materials Science and Engineering, Sungkyunkwan University, 2066, Seobu-ro, Jangan-gu, Suwon 16419, South Korea

ARTICLE INFO

Keywords:
Copper
Corrosion inhibition
Time-of-flight secondary ion mass spectrometry
Electrochemical properties

ABSTRACT

In this paper, two leaking tubes were investigated among copper tubes injected with 200 and 400 ppm benzotriazole after 8 years of usage. The electrochemical tests were conducted in simulated pit-out and pit-in environments (i.e., regions outside and inside of the pit) to determine the effect of benzotriazole on the propagation of an existing pit. The electrochemical analysis results showed that 200 and 400 ppm benzotriazole exhibit relatively lower inhibition efficiency in an acidic simulated pit-in environment because of the difficulty of forming a protective film and the benzotriazole cationization.

1. Introduction

Water leakage was the most frequent defect type encountered in buildings, and tube corrosion accounts for 50 % of leak causes [1]. As a building plumbing material, copper is widely used because of its excellent corrosion resistance property and ease of installation [2,3]. Although copper tubes provide long-term and reliable services in building plumbing, pitting corrosion induces the pinhole leakage problem [4–6]. Water leakages cause expensive damage and mold growth inside walls. In the United States, approximately 750,000 pinhole leakages occurred each year in copper tubes, and approximately US$1 billion was spent on their prevention and annual repair [4]. Building heights have increased with the development of modern technologies; hence, fire extinguishing facilities have also become increasingly important for protecting people and properties. Fire sprinkler systems are commonly used worldwide as direct fire-extinguishing facilities that reduce fire damage. Ever since South Korea enacted a law requiring sprinklers to be installed in apartments with more than 16 floors in 1992, the requirement has been expanded to include apartments with more than 6 floors until 2018 [7]. In South Korea, some construction companies have used copper, which is already widely used for building plumbing, for fire sprinkler systems. Consequently, leakages occurred due to pitting corrosion in the copper tubes of fire sprinkler systems [8,9].

Replacing all copper tubes in fire sprinkler systems is difficult because of inconvenience and high cost. Thus, suitable methods must be developed to extend the lifespan of these tubes. Corrosion inhibitors are widely used for corrosion prevention in closed systems, such as fire sprinkler systems, because the inhibitor is not lost, and only a small amount is needed [10]. Organic corrosion inhibitors are generally used for copper protection because of their higher corrosion inhibition efficiency (IE) [11,12], including azole compounds (e.g., thiazole, benzotriazole (BTAH), imidazole, and thiadiazole). BTAH is a highly effective corrosion inhibitor for copper and its alloys, even in chloride-containing environments [13–16]. It not only has low toxicity, but is also inexpensive [12]. Therefore, benzotriazole injection into installed copper tubes, where pits were initiated by deposits, carbonaceous residue, and chloric residue on the surface of the tube with sufficient oxygen in a previous study [9], has been suggested to extend the lifespan of the tubes by suppressing pit

* Corresponding author.
E-mail address: kimjg@skku.edu (J.-G. Kim).

https://doi.org/10.1016/j.heliyon.2023.e23104
Received 25 August 2023; Received in revised form 20 November 2023; Accepted 27 November 2023
Available online 30 November 2023

propagation.

From the pit initiation perspective, BTAH showed a superior IE on copper tubes in neutral tap water [17]. Also, it is a well-established fact that BTAH is highly effective in inhibiting pit initiation on copper surfaces where pits have not yet formed [18,19]. From the pit propagation perspective, it has been only reported that when BTAH was injected into copper tubes where pits had already formed, there is a possibility of BTAH entering the pit cap, and an 82 % decrease in the leakage frequency was observed for one year at 400 ppm BTAH [20,21]. However, despite that, there has been no following research conducted to analyze the causes of the ongoing leakage occurred due to pitting corrosion after BTAH injection into copper tubes where pits had already formed. These failure cases indicate the failure of BTAH to suppress the pit propagation that has already progressed significantly, rather than the pit initiation. Therefore, in this work, the effect of BTAH on the propagation of an existing pit was studied by examining two copper tubes that leaked after BTAH injection and by conducting electrochemical tests. For convenience, the uniform corrosion region outside the pit is referred to as pit-out, while the region inside the pit under the cap is referred to as pit-in. Inductively coupled plasma-optical emission spectroscopy (ICP-OES) and microstructural analysis using an optical microscope (OM) were conducted to determine the material defects in the leaking tubes. Visual inspection was performed using a stereo microscope (SM) to observe the inner tube surface and the pit structure. Surface analysis was conducted through electron probe microanalysis (EPMA), scanning electron microscopy (SEM) with energy-dispersive X-ray spectroscopy (EDS), time-of-flight secondary ion mass spectrometry (ToF-SIMS), and X-ray diffraction (XRD) on the pit-out and pit-in regions. Furthermore, the IE of BTAH on the existing pit was evaluated by electrochemical measurements, including potentiodynamic (PD) polarization tests and electrochemical impedance spectroscopy (EIS) in the simulated pit-out and pit-in environments.

2. Materials and methods

2.1. Background information

The two leaking tubes were obtained from different apartments. The sprinkler system shown in Fig. 1 was a stagnant environment pressurized with tap water. Tube No. 1 was injected with 200 ppm BTAH for the last year, with a total usage period of 9 years, by the Korea Land and Housing Corporation. Tube No. 2 was injected with 400 ppm BTAH for the last two years, with a total usage period of 10 years, also by the Korea Land and Housing Corporation. Table 1 presents the characteristics of each tube. The copper tubes had 28.58 mm diameter and 0.89 mm design thickness. The tube thicknesses were measured at eight points. The average thickness loss of each tube was calculated using the measured values. The average thickness loss of tube No. 1 over the total period of use was 0.04 mm, while that of tube No. 2 was 0.02 mm. The tubes were made of C12200 phosphorous dioxide copper according to ASTM B 75 (Table 2). ICP-OES (Agilent 5100 ICP-OES, Varian, Palo Alto, USA) was performed to compare the chemical compositions of tubes No. 1 and No. 2 with the ASTM B 75 standard.

2.2. Visual inspection and surface analysis

All tubes were cut in the axial direction for visual inspection. The pit cross-section was observed with an SM (SZ61, OLYMPUS, Tokyo, Japan) to determine the pit structure. For the microstructural analysis, the inner surface of the tubes was etched for 1 min in an alcoholic ferric chloride solution (10 g $FeCl_3$, 50 mL HCl, and 100 mL ethanol) after fine polishing. The tube microstructures were analyzed using an OM (DM2500, Leica, Wetzlar, Germany) to identify the metallurgical impurities and precipitates. The surface morphology was observed through SEM (JSM-6700F, JEOL Ltd., Tokyo, Japan). The surface components were analyzed through EPMA (JXA-8530F, JEOL Ltd., Tokyo, Japan). In addition, EDS (JSM-6700F, JEOL Ltd., Tokyo, Japan) was conducted to compare the surface component differences between the pit-out and pit-in regions. The positive static ToF-SIMS (ToF-SIMS V, ION-TOF, Münster, Germany) was conducted to analyze the molecular and elemental compositions of the surfaces of the leaking copper tubes. The ToF-SIMS spectra were obtained using a pulsed 30 keV Bi^+ primary ion source over a 300 μm × 300 μm area. The XRD (SmartLab, Rigaku, Tokyo, Japan)

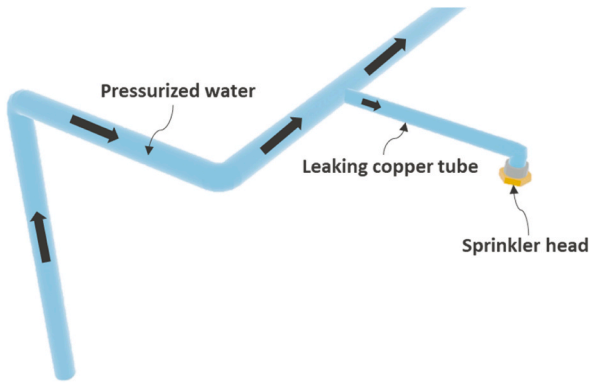

Fig. 1. Schematic diagram of a leaking copper tube in a sprinkler system.

Table 1
Characteristics of the leaking copper tubes injected with 200 and 400 ppm BTAH.

Tube	BTAH concentration (ppm)	Average thickness loss (mm)	Period of use (year)	Period of BTAH injection (year)
No. 1	200	0.04	9	1
No. 2	400	0.02	10	2

Table 2
Standard chemical composition of the C12200 copper tube in ASTM B 75 (wt.%).

C12200, ASTM B 75		
Chemical composition (wt. %)	Cu	99.9 min
	P	0.015–0.040

measurements were performed to identify the corrosion product. The XRD analysis was conducted with a Cu Kα radiation source. The wavelength was approximately 1.54 Å in the 2θ range of 5–90° at a 0.02°/s scan rate.

2.3. Electrochemical analysis

For the electrochemical measurements, the as-received C12200 copper tube was cut to 1.5 cm × 1.5 cm. All specimens were polished with a 600-grit silicon carbide paper, rinsed with ethanol, and finally dried with nitrogen gas. The corrosion environment was synthetic tap water (Table 3) based on the actual tap water composition. The pH of the solutions was adjusted by using extra pure-grade reagent nitric acid (HNO_3). Electrochemical tests were performed to compare the inhibition properties according to the BTAH concentrations of 0, 200, 400, and 1000 ppm in the simulated pit-out and pit-in environments. Fig. 2 illustrates the propagation of the sprinkler copper tube pit. In the space under the mound-shaped oxide cap, the pit propagated because of the formation of an oxygen concentration cell and a harsh environment with low pH and high Cl^- concentration [8,22,23]. The acidic chloride electrolyte inside the underdeposit pit can reach the pH of the saturated metal-salt solution [24]. The saturated $CuCl_2$ solution was prepared, and its pH was measured at 0.25 using a pH meter (ORION STAR A111, Thermo Fisher Scientific, Waltham, United States). In particular, pH is known to have a large effect on the IE of BTAH [25–27]. Therefore, the electrochemical experiments were conducted by setting the pH of the synthetic tap water to pH 7.1 and 0.25 for the simulated pit-out and pit-in environments, respectively, to confirm the effect of environmental differences on the IE of BTAH.

All the electrochemical experiments were conducted in a three-electrode system using the specimen as the working electrode, a graphite rod as the counter electrode, and a saturated calomel electrode (SCE) as the reference electrode. The area exposed to the electrolyte was 1 cm^2. After all specimens had been immersed in the synthetic tap water solution for 24 h, the PD and EIS tests were performed with a multi-potentiostat/galvanostat model VSP-300. The PD tests and EIS were conducted to examine the IE of BTAH in the simulated environments (pit-out and pit-in). Following ASTM G5, the PD tests were executed with a potential sweep of 0.166 mV/s in a potential range of −250 mV vs. open-circuit potential (OCP) to 1000 mV vs. OCP. EIS was performed at 10 mV amplitude in the frequency range from 100 kHz to 10 mHz. The impedance plots were interpreted based on the equivalent circuit using an appropriate fitting procedure by ZsimpWin software.

3. Results and discussion

3.1. Metallurgical analysis

Table 4 shows the chemical compositions of tubes No. 1 and No. 2 measured by ICP-OES. The P content specification of C12200 was between 0.015 and 0.040 wt%. Both pipes satisfied the P content specification. Accordingly, 0.002 wt% C and 0.00082 wt% Fe were detected in tube No. 1 and 0.00091 wt% Fe was detected in tube No. 2. The C and Fe contents comprised small amounts of alloy impurities incorporated into the material during the manufacturing process. Consequently, tubes No 1. and No. 2 had 99.96 wt% and 99.958 wt% Cu, both satisfying the ASTM B 75 standard.

Fig. 3(a and b) shows the microstructures of the inner surface of the tubes observed using an OM. The microstructures of both leaking copper tubes are typical of drawn copper. The grains of copper tubes wrought through the drawing process are elongated in shape along the longitudinal direction due to the deformation. In addition, no defects, pores, precipitates, or impurities were observed in the microstructure.C12200 is a commercially pure copper that contains less P content than the solid solubility limit; hence, no precipitates were formed. The ICP-OES and OM results showed no issues regarding the chemical composition and microstructure of

Table 3
Chemical composition of the synthetic tap water for the electrochemical measurements (mol/dm^3).

Mg^{2+}	Ca^{2+}	SO_4^{2-}	Cl^-
5.31×10^{-7}	1.29×10^{-6}	1.37×10^{-7}	4.45×10^{-7}

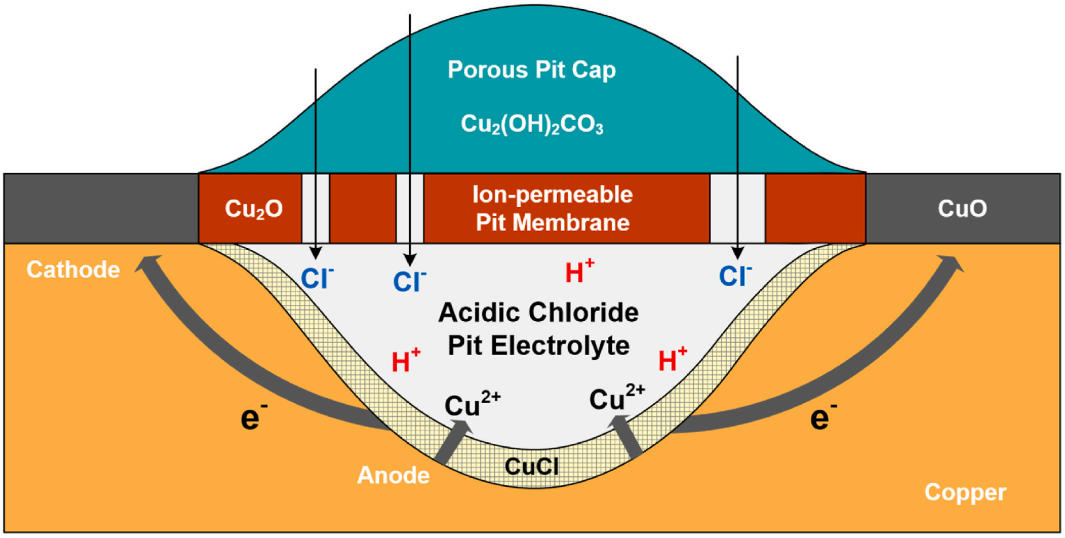

Fig. 2. Schematic diagram of the pit propagation mechanism in a sprinkler copper tube.

Table 4
Chemical composition of the leaking copper tubes measured by ICP-OES (wt.%).

Tube	Cu	C	P	Fe
No. 1	99.96	0.002	0.0342	0.00082
No. 2	99.958	–	0.0408	0.00091

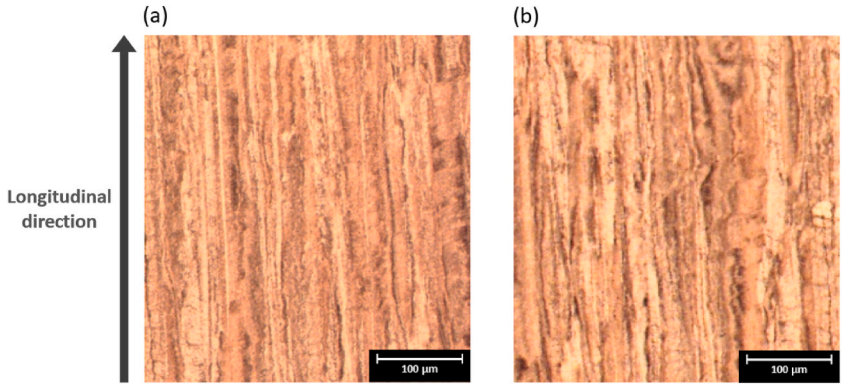

Fig. 3. Microstructures of the inner surface of the leaking copper tubes filled with (a) 200 ppm BTAH (No. 1) and (b) 400 ppm BTAH (No. 2).

both tubes.

3.2. Visual inspection

Both tubes had a small average thickness loss, indicating a slow progression of a uniform corrosion. Nevertheless, several pits were formed in tubes No. 1 and No. 2, leading to leaks. Fig. 4(a and b) shows the inner surface of the copper tubes cut in the longitudinal direction. Several pits (white arrows) lined up in the longitudinal direction were observed on the inner surface of both tubes. Tube No. 1 was uniformly covered with black oxide, while tube No. 2 was partially covered with black oxide. A blue-green oxide formed by the locally accelerated corrosion in the pit was also observed in the pits of tubes No. 1 and No. 2 [28]. Fig. 5(a and b) shows the cross-section of pit structure. A mound-shaped cap was present above the pit in both tubes. A space and an ion-permeable pit membrane existed inside the cap. This is the typical shape of pitting corrosion on copper, which is accompanied by the mound-shaped cap in general sprinkler copper tubes not filled with BTAH [8,9].

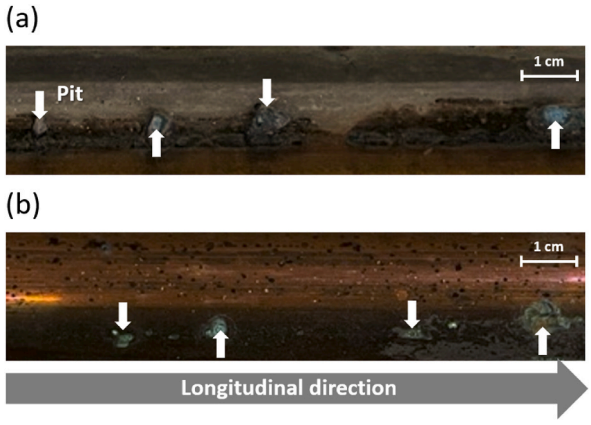

Fig. 4. Images of the inner surfaces of the tubes in the longitudinal direction: (a) No. 1 and (b) No. 2.

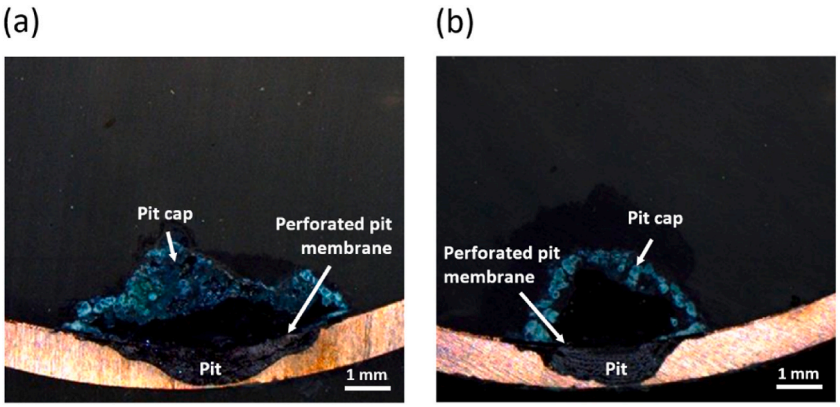

Fig. 5. Cross-section images of the pits of the leaking tubes filled with (a) 200 ppm BTAH (No. 1) and (b) 400 ppm BTAH (No. 2).

3.3. Surface analysis

In the case where BTAH was filled after the pit was formed, EPMA mapping was performed on the pit-out region to produce a first view of the inner surface components of the tubes. Fig. 6(a) shows the SEM and EPMA mapping results on the pit-out region of tube No. 1. The SEM and EPMA mapping of the O and Cu elements showed that oxides were formed all over the pit-out region. The regions with high Cl concentration, which accelerates local corrosion of copper, were seen [29–31]. C, N, and H compose the molecular structure of BTAH. H is difficult to detect through EPMA mapping, but the presence of BTAH can be confirmed by mapping C and N elements. A small amount of N was detected on the pit-out region of tube No. 1. The presence of BTAH was confirmed because C and N elemental mappings corresponded, especially in the white circles. Fig. 6(b) shows that copper oxide was formed on the pit-out region of tube No. 2, as observed for tube No. 1. This could be CuO and Cu_2O, which were generally formed on the surface of the copper tubes, which are well known to act as protective layers against copper corrosion [4,9]. The region with a high Cl concentration was not clearly visible in the mapping area of tube No. 2. The corresponding mappings of C and N elements verified the presence of BTAH on the pit-out region of tube No. 2, particularly in the white circles.

Fig. 7(a and b) shows the surface images of the pit after the cap for each tube was removed. Surface analysis was performed at the places marked with yellow boxes, where A and B denote the pit-out and pit-in regions, respectively. Black oxide was uniformly formed in A of both tubes. Dark red and blue-green oxides were visible in B, and copper was exposed below them. Fig. 8(a) and (b) show the surface SEM results from A of No. 1. The spherical copper oxides were uniformly formed in A of No. 1 [9]. In addition, at a high magnification, surface deposits with a jagged shape were uniformly formed on CuO and Cu_2O. These are similar to those that occurred when BTAH formed a protective film on copper in a Cl^- environment [32]. Fig. 8(c) and (d) show the surface SEM results from B of tube No. 1. The surface deposits were not identified in B of tube No. 1, but very coarse cubic Cu_2O and bare copper surfaces were observed [9]. Fig. 8(e) and (f) demonstrate the surface SEM results from A of tube No. 2, confirming that spherical CuO and Cu_2O were uniformly formed as in A of tube No. 1. The surface deposits with a jagged shape were also more densely and uniformly formed because of the higher BTAH concentration in tube No. 2 compared to that in tube No. 1. Fig. 8(g) and (h) illustrate the surface SEM results from B of tube No. 2. Only coarse cubic Cu_2O and bare copper surfaces were observed without surface deposits the same as B of tube No. 1.

EDS analysis was performed from each box area in Fig. 8 to confirm the difference between the pit-out and pit-in surface

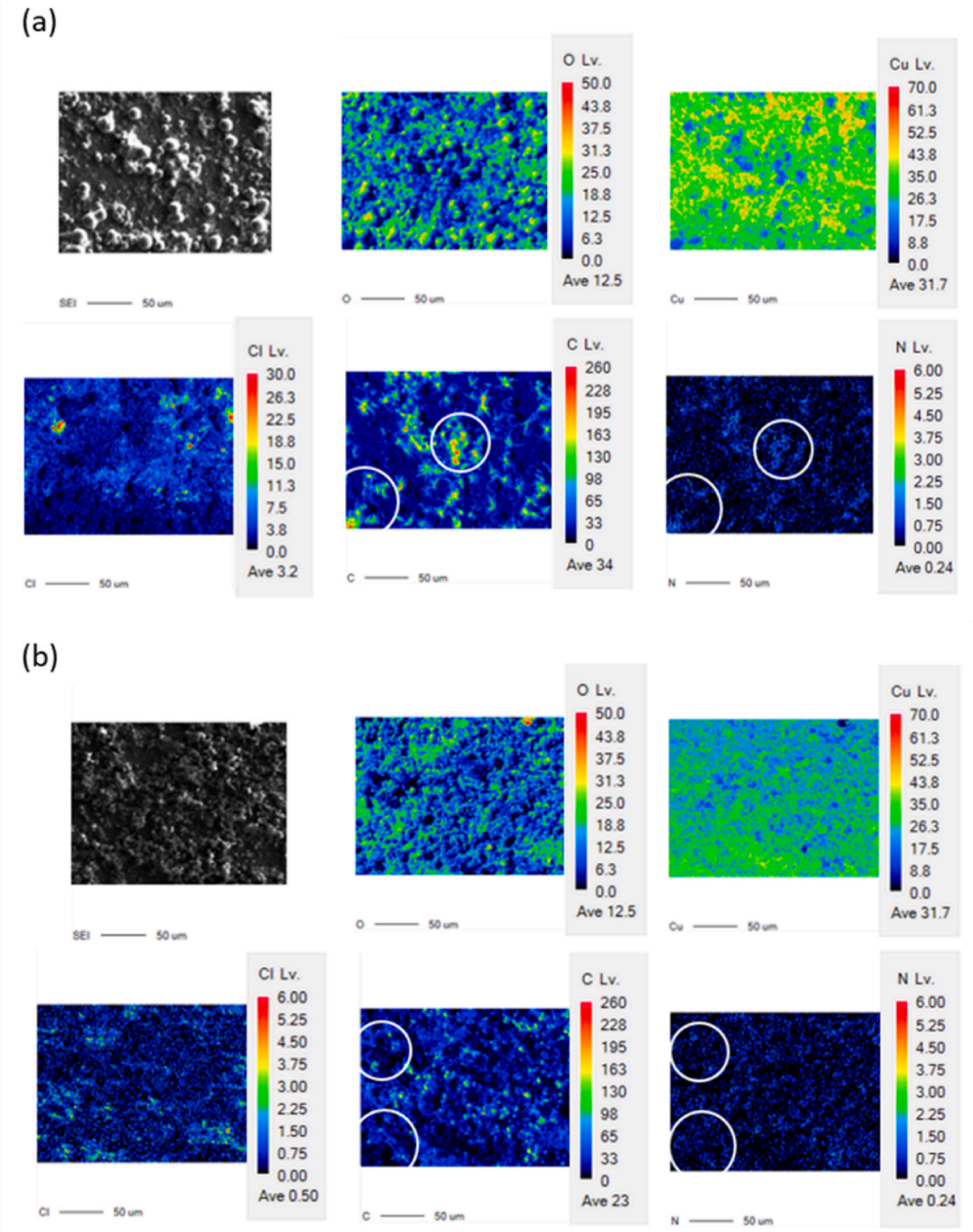

Fig. 6. SEM and EPMA mapping results of pit-out regions of the leaking copper tubes filled with (a) 200 ppm BTAH (No. 1) and (b) 400 ppm BTAH (No. 2).

compositions. Table 5 presents the EDS results. The Cu, O, C, and N elements were detected in A of tube No. 1. This finding confirmed the presence of CuO and BTAH, which were consistent with the SEM results. Only the Cu and O elements were detected in B of tube No. 1. This was considered to be Cu_2O, and the exposed copper surface identified in the SEM results. Unlike in A, C and N were not detected, and BTAH was not uniformly adsorbed in B. Similar to the results of tube No. 1, the Cu, O, C, and N elements were detected in A of tube No. 2. This result was similar to that obtained by SEM, indicating that CuO and BTAH existed. In B of tube No. 2, the C and N elements were not detected, but the Cu, O, and Cl elements were detected. As for B of tube No. 1, BTAH was not uniformly adsorbed in B of tube No. 2. Cl^- was concentrated in B of tube No. 2 during the pit propagation and formed CuCl [8,33]. The following reactions occur during the pit propagation in the sprinkler copper tube [8,34,35]:

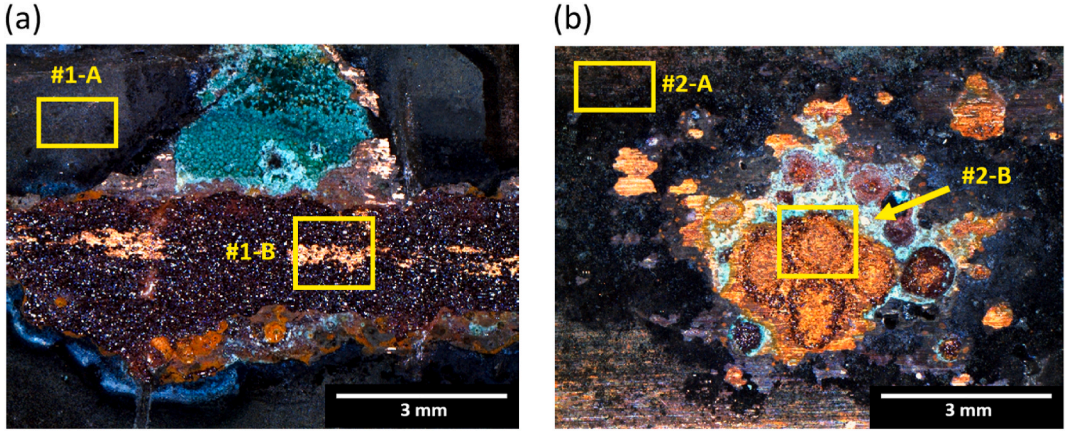

Fig. 7. Surface images of the pit after cap removal: (a) No. 1 and (b) No. 2.

Reactions occur in the pit-in region as per Eqs. (1) and (2):

$$Cu + Cl^- \rightarrow CuCl + e^- \quad (1)$$

$$2CuCl + H_2O \rightarrow Cu_2O + 2H^+ + 2Cl^- \quad (2)$$

Cu_2O of Eq. (2) form the membrane and it is dissolved because of acidic environment. Thus, reaction occurs on the inner surface of the membrane as per Eq. (3):

$$Cu^+ \rightarrow Cu^{2+} + e^- \quad (3)$$

Cu^{2+} can diffuse to the pit-out region, which is locally alkaline because of cathodic reaction. Therefore, following Eq. (4) occurs within the cap above pit:

$$2Cu^{2+} + 2OH^- + CO_3^{2-} \rightarrow + Cu_2(OH)_2CO_3 \quad (4)$$

Eq. (2) produced Cl^-, which led to an anodic reaction on the copper tube surface in the pit-in region and repeatedly formed CuCl. The reaction also produced H^+; hence, the pit-in region gradually became an acidic environment as the reaction continued to repeat.

Fig. 9 depicts the molecular structure of BTAH, a heterocyclic compound that features a five-membered ring containing three nitrogen atoms. Fig. 10(a–d) shows the ToF-SIMS spectra obtained from the pit-out and pit-in regions. Copper has two main isotopes at *m/z* 62.92 for $^{63}Cu^+$ and *m/z* 64.92 for $^{65}Cu^+$ obtained in the ToF-SIMS spectra. Table 6 shows the ToF-SIMS analysis results of the positive ions related to BTAH. The ToF-SIMS spectra contained various hydrocarbon-related fragments (Table 6) caused by the fragmentation of the BTAH molecules. The signal for $C_6H_5^+$ was equivalent to the phenyl cation and closely related to the benzene ring [36]. These signals for $C_6H_5N^+$ and $C_6H_5N_2^+$, which contained nitrogen, most likely originated in the BTAH fragmentation. Meanwhile, the signal for $C_6H_5N_3^+$ verified the presence of the BTAH molecules on the surface. The above-mentioned signals for BTAH and its fragments were detected in both the pit-out and pit-in regions of tubes No. 1 and No. 2. The ToF-SIMS results provided evidence that BTAH existed in the pit-out and pit-in regions of both tubes. The signal for $C_6H_5N_3Cu^+$ corresponding to the BTAH–Cu organometallic complex was also detected under all conditions. Unlike the EDS measurements, the ToF-SIMS measurements showed that BTAH was present in the pit-in region because ToF-SIMS generally had better detection limits and spatial resolution than EDS [37]. From the ToF-SIMS measurements, the BTAH adsorption can be demonstrated with considerable confidence because the detection of a particular molecule is certain compared to EDS, which can determine only the presence of the C and N elements. As a result, although BTAH was also adsorbed on the pit-in regions of tubes No. 1 and No. 2, the protective films were not fully formed because BTAH was not sufficiently adsorbed on the pit-in surface, in contrast to the pit-out surface.

XRD was performed on the pit-out and pit-in regions of tubes No. 1 and No. 2. Fig. 11(a) shows the XRD results from the pit-out region of tubes No. 1 and No. 2. CuO and Cu_2O peaks, which are generally observed in fire-extinguishing sprinkler tubes, were detected in the pit-out region [8,9]. These oxides are known to act as protective films on the copper surface. Fig. 11(b) shows the XRD results from the pit-in region of tubes No. 1 and No. 2. CuCl, $Cu(OH)_2$, $CuCO_3$, $Cu_2(OH)_2CO_3$, and $Cu_4(OH)_6SO_4$–H_2O were observed in the pit-in region beside CuO and Cu_2O. These oxides formed in the copper pit [28,33,38]. As determined by EDS, CuCl was observed in the pit-in region. The CuCl formation supported the Cl^- concentration under the oxide mound during the pit propagation.

3.4. Electrochemical analyses

3.4.1. PD polarization tests

Fig. 12(a and b) shows the PD polarization curves of the copper tubes in the simulated pit-out environment at pH 7.1 (a) and the simulated pit-in environment at pH 0.25 (b). Both polarization curves shifted to the left as the BTAH concentration increased because

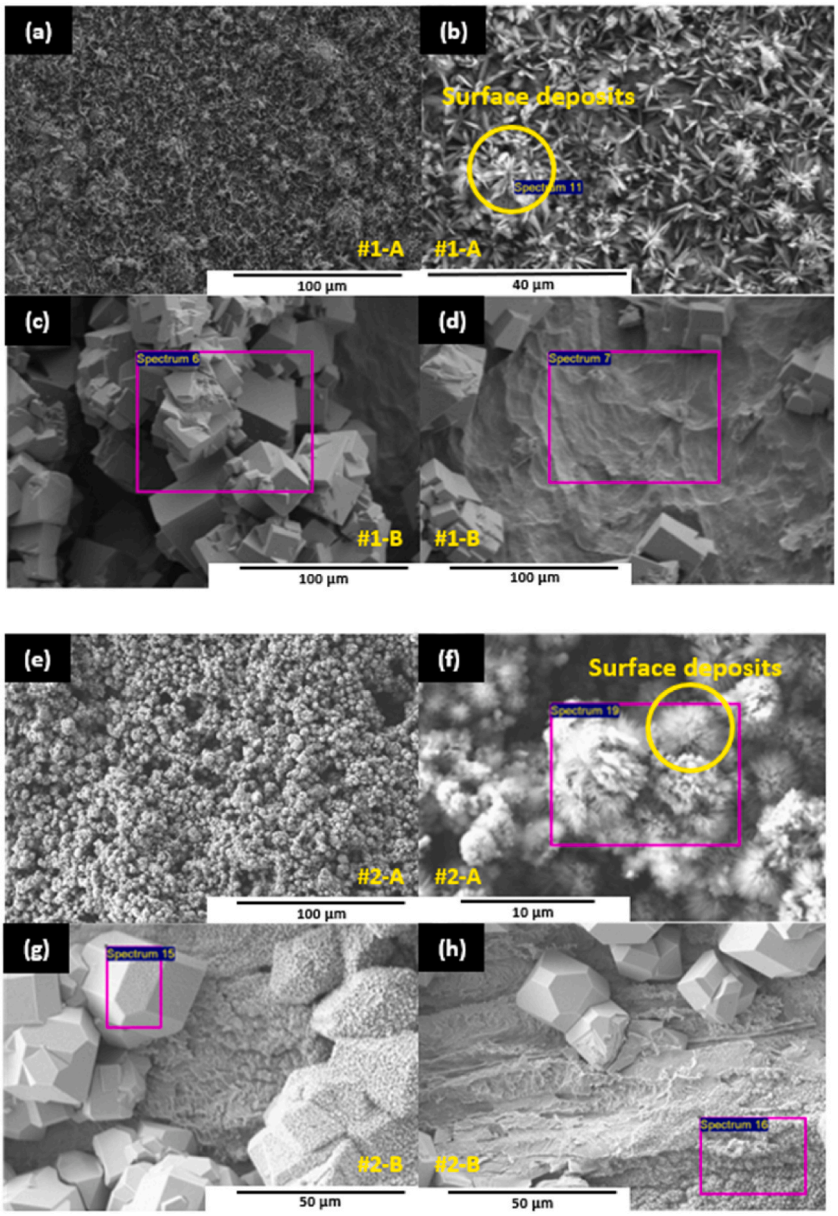

Fig. 8. SEM results from (a, b) A (pit-out) of No. 1, (c, d) B (pit-in) of No. 1, (e, f) A of No. 2, and (g, h) B of No. 2.

Table 5
EDS results obtained from the boxes in Fig. 8 (wt.%).

Element Fig. 8	C	N	Cl	O	Cu	Total
(b)	36.23	20.17	–	7.15	36.45	100.00
(c)	–	–	–	11.79	88.21	100.00
(d)	–	–	–	–	100.00	100.00
(f)	26.58	18.44	–	17.37	37.61	100.00
(g)	–	–	12.84	21.48	65.68	100.00
(h)	–	–	16.72	24.71	58.58	100.00

BTAH was adsorbed on the copper surface and acted as a mixed inhibitor of both the anodic and cathodic reactions [12,25,32]. When a mixed inhibitor is added, the corrosion potential of the metal shifts depending on which half-cell reaction is more affected. The tendency for E_{corr} to increase as the concentration of BTAH increases at pH 7.1 indicates that the anodic reaction is more inhibited than

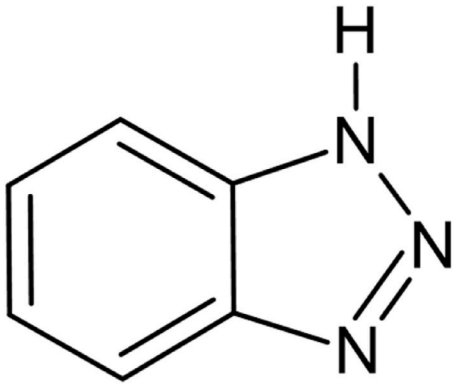

Fig. 9. Molecular structure of BTAH ($C_6H_5N_3$).

the cathodic reaction. Conversely, the tendency for E_{corr} to decrease as the concentration of BTAH increases at pH 0.25 indicates that the inhibition of the cathodic reaction was greater than the inhibition of the anodic reaction. Also, the polarization curves of the copper tube also showed a passive behavior with the addition of BTAH. However, the passive behavior was unstable in the simulated pit-in environment unlike the simulated pit-out environment. The breakdown potential (E_b) is the potential at which the passive film breaks down and improved as the BTAH concentration increased. This passive behavior was due to the BTAH adsorption on the copper surface, which formed the Cu–BTA film that acted as a physical barrier to the aggressive ion diffusion [39,40]. The barrier broke when the surface exceeded a certain potential E_b, and pitting corrosion initiated at the broken part.

The electrochemical parameters were obtained from the PD polarization curves conducted at least two times (Table 7). i_{corr} and the corrosion rate decreased as the BTAH concentration increased for both pH 7.1 and 0.25. The IE was calculated as per Eq. (5) using the corrosion current density without the inhibitor, i^0_{corr}, and the corrosion current density with the inhibitor, i_{corr} [32,41]:

$$IE\ (\%) = \left[\frac{\left(i^0_{corr} - i_{corr}\right)}{i^0_{corr}}\right] \times 100 \tag{5}$$

Fig. 13(a and b) shows the IE and ($E_b - E_{corr}$) as the line graphs to examine the effect of the pH value between the pit-out and pit-in simulated environments on the IE and the stability of the Cu–BTA film. The IE of the 200 ppm BTAH increased by from 48 % at pH 0.25–90 % at pH 7.1. Even 400 ppm BTAH, the IE increased from 70 % at pH 0.25–92 % at pH 7.1. The ($E_b - E_{corr}$) value was 3.9 times smaller at pH 0.25 (100 mV_{SCE}) compared to 385 mV_{SCE} at pH 7.1 for the 200 ppm BTAH. For the 400 ppm BTAH, the value was 2.5 times smaller at pH 0.25 (210 mV_{SCE}) compared to 525 mV_{SCE} at pH 7.1. These results showed that injecting 200 and 400 ppm BTAH after the pit formation in tubes No. 1 and No. 2 could not form the passive film sufficient enough to suppress the corrosion inside the pit. Consequently, the leakage occurred as the pit propagated in tubes No. 1 and No. 2. However, the IE and ($E_b - E_{corr}$) increased as the BTAH concentration increased in both simulated environments. In the simulated pit-out environment, the IE and ($E_b - E_{corr}$) value of 1000 ppm BTAH increased to 97 % and 625 mV_{SCE}, respectively. Even in the simulated pit-in environment, the IE and ($E_b - E_{corr}$) value of 1000 ppm BTAH increased to 82 % and 235 mV_{SCE}, respectively. Therefore, BTAH must be injected with a concentration higher than 1000 ppm to prevent the pit propagation in the copper tubes.

3.4.2. EIS measurements

Fig. 14(a and b) shows the Nyquist plots obtained for the copper tubes as a function of the BTAH concentration in the simulated (a) pit-out (pH = 7.1) and (b) pit-in (pH = 0.25) environments. Regardless of the pH, the capacitive loop radius increased as the BTAH concentration increased. However, the loops were larger at pH 7.1 than at pH 0.25. This indicated that the corrosion suppression ability of BTAH in the simulated pit-in environment was lower than that in the simulated pit-out environment. The equivalent circuit shown in Fig. 15 was used to fit the EIS results without and with BTAH [42,43]. The time constant associated with the relaxation process of the electrical double layer was dominant in this circuit because the obtained $R_{barrier}$ was the sum of the electrical double layer and adsorption layer effects and cannot be separated. In other words, BTAH formed a physical barrier that protected the metal from corrosive ions [39,44]. In Fig. 15, R_s is the solution resistance, and R_{ct} is the result of the ion conduction path formation caused by the barrier defects or pores. The CPE was applied instead of an ideal capacitance C_{dl} with a varying n to attain a more accurate fit. The CPE impedance is expressed as the following Eq. (6) [45,46]:

$$Z_{CPE} = A^{-1}(i\omega)^{-n} \tag{6}$$

where, A is the CPE magnitude; i is the imaginary number ($i^{-2} = -1$); ω is the sine wave modulation angular frequency; and n is the empirical parameter ($0 \leq n \leq 1$) measured for the deviation from the ideal capacitive behavior.

Table 8 presents the impedance parameters obtained from the EIS data conducted at least two times. The IE was calculated as the following Eq. (7) using the EIS results to verify the reliability of the PD polarization results (ion conduction path resistance without the inhibitor, R^0_{ct}, and ion conduction path resistance with the inhibitor, R_{ct}) [39]:

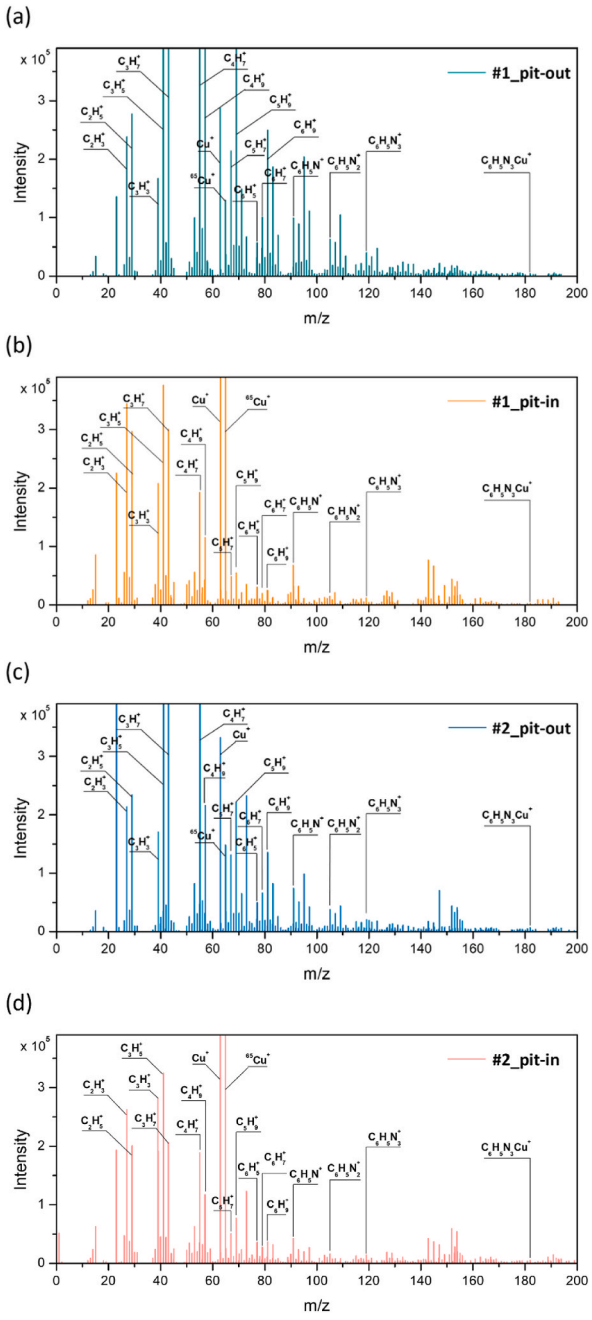

Fig. 10. ToF-SIMS surface positive ion mass spectra obtained from the (a) pit-out region of tube No. 1, (b) pit-in region of tube No. 1, (c) pit-out region of tube No. 2, and (d) pit-in region of No. 2.

$$IE(\%) = \left[\frac{\left(R_{ct} - R_{ct}^{0}\right)}{R_{ct}}\right] \times 100 \tag{7}$$

In both simulated environments, R_{ct} and the IE increased as the BTAH concentration increased. However, R_{ct} and the IE showed significant differences between the pit-out and pit-in simulated environments. This supported the PD polarization results and demonstrated that the effect of BTAH as an inhibitor is inferior in the acidic pit-in environment. The CPE decreased as the BTAH concentration increased in both simulated environments and was larger in the simulated pit-in environment than in the simulated pit-out environment. The CPE was inversely proportional to the physical barrier thickness [47]. Thus, the physical barrier thickness increased as the BTAH concentration increased. The barrier thickness was also thinner in the simulated pit-in environment than in the simulated pit-out environment.

Table 6
ToF-SIMS analysis results of the positive ions related to BTAH obtained from the pit-out and pit-in regions of tubes No. 1 and No. 2.

m/z	Chemical formula	Peak assignment
27.02	$C_2H_3^+$	Hydrocarbon-related fragments
29.04	$C_2H_5^+$	
39.02	$C_3H_3^+$	
41.04	$C_3H_5^+$	
43.05	$C_3H_7^+$	
55.05	$C_4H_7^+$	
57.07	$C_4H_9^+$	
67.05	$C_5H_7^+$	
69.08	$C_5H_9^+$	
77.03	$C_6H_5^+$	
79.05	$C_6H_7^+$	
81.06	$C_6H_9^+$	
91.04	$C_6H_5N^+$	Fragments containing nitrogen atom
105.06	$C_6H_5N_2^+$	
119.03	$C_6H_5N_3^+$	BTAH
181.95	$C_6H_5N_3Cu^+$	BTAH–Cu

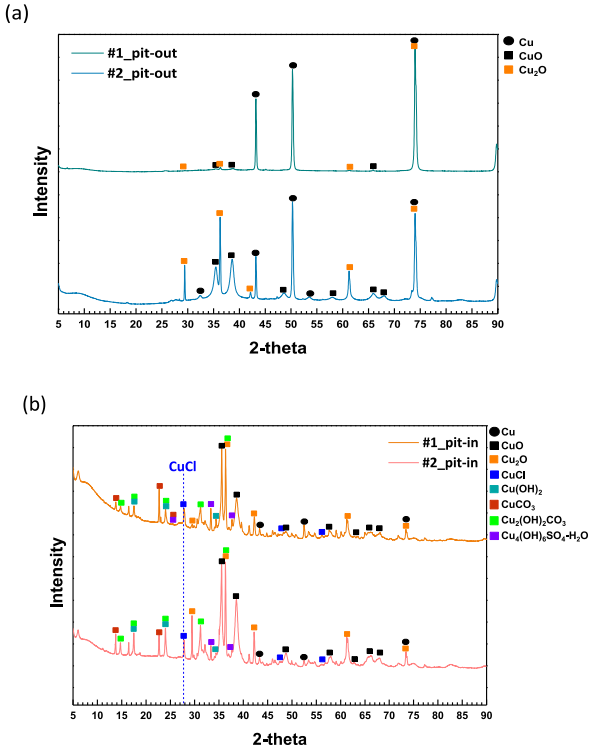

Fig. 11. XRD results obtained from the (a) pit-out and (b) pit-in regions of tubes No. 1 and No. 2.

The electrochemical analysis results supported the finding that the effect of BTAH as an inhibitor on the copper tubes is affected by the acidic pit-in environment. The reduction in the IE of BTAH in the acidic environment can be explained by the Cu−BTAH film formation and the soluble forms of BTAH. In an environment where Cl^- ions are present, BTAH forms a protective film on the copper surface through the following reactions [12,48,49]:

$$Cu + BTAH \rightarrow (Cu - BTAH)_{ads} \tag{8}$$

$$nCuCl_2^- + nBTAH \rightarrow (CuBTA)_n + nH^+ + 2nCl^- \tag{9}$$

$$(Cu - BTAH)_{ads} + (CuBTA)_n \rightarrow \left[(Cu - BTAH) - (CuBTA)_n\right]_{ads} \tag{10}$$

For BTAH to form a protective film, Eqs. (8)–(10) should sequentially occur. However, the reaction occurred in the reverse

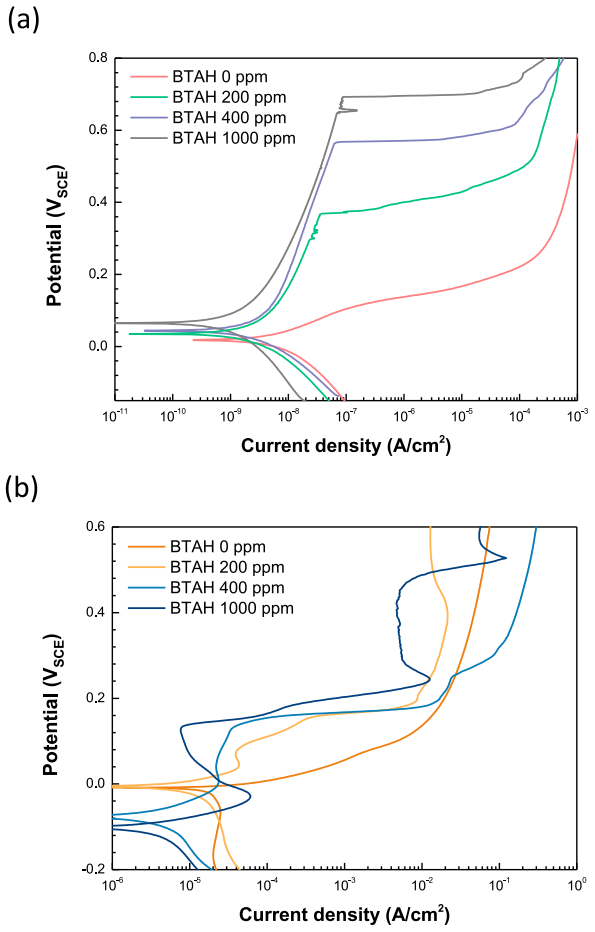

Fig. 12. PD polarization curves of the copper tubes in the synthetic tap water at 25 °C as a function of the BTAH concentration in the simulated (a) pit-out (pH = 7.1) and (b) pit-in (pH = 0.25) environments.

Table 7
Electrochemical parameters obtained from the PD polarization curves of the copper tubes in the synthetic tap water as a function of the pH and BTAH concentration.

pH	C_{BTAH} (ppm)	E_{corr} (mV_{SCE})	i_{corr} (A/cm^2)	Corrosion rate (μm/year)	IE (%)	$E_b - E_{corr}$ (mV_{SCE})
7.1	0	26	1.4×10^{-8}	0.16	–	–
	200	34	1.4×10^{-9}	0.016	90 (±1.4)	385 (±77.8)
	400	38	1.1×10^{-9}	0.012	92 (±0.71)	525 (±7.07)
	1000	48	3.7×10^{-10}	0.0043	97 (±0.71)	625 (±7.07)
0.25	0	−29	1.4×10^{-5}	163	–	–
	200	−31	7.3×10^{-6}	85	48 (±3.5)	100 (±28.3)
	400	−78	4.2×10^{-6}	48	70 (±3.5)	210 (±14.1)
	1000	−101	2.5×10^{-6}	29	82 (±1.4)	235 (±7.07)

direction, where $(CuBTA)_n$ was dissolved according to Eq. (9), because the inside of the pit had high H^+ and Cl^- concentrations. Therefore, it was difficult for BTAH to form a protective film, which was consistent with the PD polarization and EIS results. In the acidic environment, the IE of BTAH was reduced because the soluble form differed from that in the neutral environment. BTAH is known to have three soluble forms depending on the solution pH: BTAH, $BTAH_2^+$, and BTA^-. The changes occurred according to the following Eqs. (11) and (12) [48,50]:

$$BTAH_2^+ \leftrightarrow BTAH + H^+, pk_1 \approx 1 \tag{11}$$

$$BTAH \leftrightarrow BTA^- + H^+, pk_2 \approx 8.2 \tag{12}$$

In Eq. (11), BTAH is protonated to $BTAH_2^+$ when the pH is less than 1. The cationization to $BTAH_2^+$ makes it difficult to produce the

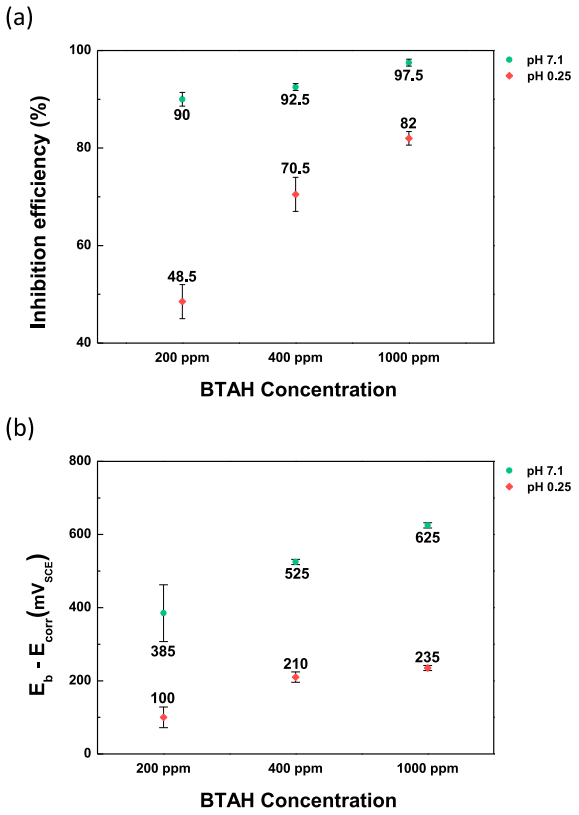

Fig. 13. Line graphs from the PD polarization results of the copper tubes as a function of the pH and BTAH concentration: (a) IE and (b) $E_b - E_{corr}$.

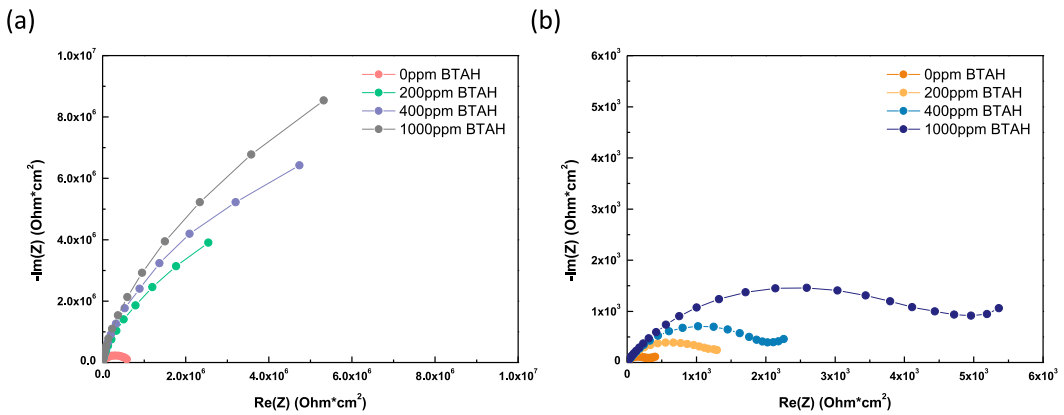

Fig. 14. Nyquist plots for the copper tubes as a function of the BTAH concentration in the simulated (a) pit-out (pH = 7.1) and (b) pit-in (pH = 0.25) environments.

initial monolayer corresponding to Eq. (8).

Finally, we can deduce that BTAH did not form a protective film in the pit-in region of tubes No. 1 and No. 2 because of the environmental influences considering that the pH in the pit-in environment could reach 0.25 when the pit already formed. The high Cl^- concentration during pit propagation was also expected to reduce the IE of BTAH due to dissolving the $(CuBTA)_n$ according to Eq. (9). However, this study was first conducted intensively on the pH as a single factor that greatly affects the IE of BTAH. Also, the presence of water remaining in the tubes after drainage can lead to a reduced effectiveness of the injected BTAH in inhibiting pit propagation, as the concentration of the BTAH may become lower than intended. It is important to consider this factor when injecting BTAH into tubes that are already in use.

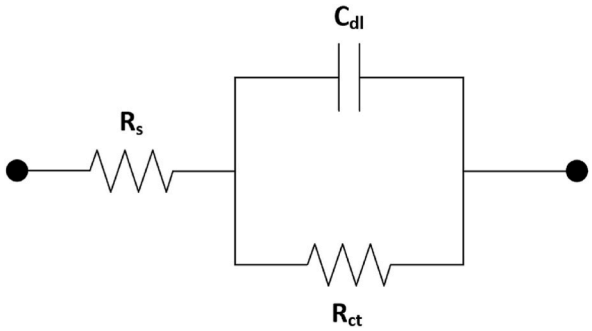

Fig. 15. Equivalent circuit for the EIS result fitting for the copper tube as a function of the BTAH concentration in the simulated pit-out and pit-in environments.

Table 8
Impedance parameters obtained from the EIS measurements of the copper tubes as a function of the pH and BTAH concentration.

pH	C_{BTAH} (ppm)	R_s (Ω-cm^2)	$CPE1$ (F/cm^2)	n_1	R_{ct} (Ω-cm^2)	IE (%)
7.1	0	1.03×10^3	2.88×10^{-6}	0.876	5.40×10^5	–
	200	1.20×10^3	2.52×10^{-6}	0.916	8.59×10^6	94 (±0.7071)
	400	1.04×10^3	1.52×10^{-6}	0.931	1.33×10^7	96 (±0.7071)
	1000	6.30×10^2	1.28×10^{-6}	0.932	1.69×10^7	97 (±0.0007)
0.25	0	1.29	8.40×10^{-4}	0.765	4.45×10^2	–
	200	1.64	7.07×10^{-4}	0.737	1.20×10^3	63 (±4.2426)
	400	0.56	2.18×10^{-4}	0.776	2.30×10^3	81 (±0.7071)
	1000	5.56	1.16×10^{-4}	0.749	4.89×10^3	91 (±0.0004)

4. Conclusions

This study investigated the effect of BTAH as a corrosion inhibitor on an already-formed pit through the failure analysis of copper tubes that leaked after BTAH injection, and the electrochemical analyses based on the BTAH concentration in simulated pit-out and pit-in environments. The following conclusions were obtained in this work.

- ICP-OES and microstructural analysis indicated no metallurgical problems in tubes No. 1 and No. 2. A number of pits accompanied by an oxide cap in a mound shape were also confirmed through the surface and cross-section observations of both tubes.
- SEM, EPMA, EDS, and ToF-SIMS results verified that BTAH was adsorbed on the pit-out region and formed a protective film. By contrast, it was unevenly present inside of the pit surface, and the Cl^- ions were concentrated in the pit-in region based on EDS and ToF-SIMS.
- The pH value could reach 0.25 in the pit-in region under a mound-shaped oxide cap unlike in the pit-out region. The PD and EIS results showed that the simulated pit-in environment decreased the IE and $E_b - E_{corr}$ of BTAH. Thus, in some copper tubes with a much-propagated pit, 200 and 400 ppm BTAH did not sufficiently suppress the pit propagation because of the relatively lower IE in the pit-in region. This led to a leakage in both investigated tubes.
- PD and EIS results showed that the IE and $E_b - E_{corr}$ of BTAH increased with the BTAH concentration in both simulated pit-out and pit-in environments. Therefore, injecting a sufficiently high BTAH concentration above 1000 ppm is recommended to suppress the pit propagation.

Data Availability

Data will be made available on request.

CRediT authorship contribution statement

Eun-Ha Park: Writing - original draft, Investigation, Formal analysis, Data curation, Conceptualization. **Sang-Jin Ko:** Writing - review & editing, Project administration, Formal analysis. **Jung-Gu Kim:** Writing - review & editing, Project administration.

Declaration of competing interest

The authors declare the following financial interests/personal relationships which may be considered as potential competing interests:Jung-Gu Kim reports financial support was provided by Korea Land and Housing Corporation.This research was supported by the SungKyunKwan University and the BK21 FOUR(Graduate School Innovation) funded by the Ministry of Education(MOE, Korea)

and National Research Foundation of Korea(NRF).

References

[1] M. Chew, Defect analysis in wet areas of buildings, Construct. Build. Mater. 19 (3) (2005) 165–173.
[2] Z. Jia, et al., Analysis of copper pitting failure in drinking water distribution system, J. Fail. Anal. Prev. 11 (2) (2011) 152–157.
[3] O. Farooqi, et al., Copper pinhole failures: plumbing susceptibility and management, J. Water Resour. Plann. Manag. 135 (4) (2009) 227–236.
[4] J. Gibson, B. Karney, A 30-year review of copper pitting corrosion and pinhole leaks: Achievements and research gaps, AWWA Water Science 3 (2) (2021) e1221.
[5] D.B. Harrison, D.M. Nicholas, G.M. Evans, Pitting corrosion of copper tubes in soft drinking waters: corrosion mechanism, J. Am. Water Works Assoc. 96 (11) (2004) 67–76.
[6] S.H. Lee, J.G. Kim, J.Y. Koo, Investigation of pitting corrosion of a copper tube in a heating system, Eng. Fail. Anal. 17 (6) (2010) 1424–1435.
[7] Enforcement ordinance for firefighting facilities, Maintenance and Safety Management of Korea, 2022.
[8] S.H. Suh, et al., Analysis of pitting corrosion failure of copper tubes in an apartment fire sprinkler system, Eng. Fail. Anal. 64 (2016) 111–125.
[9] S.J. Ko, et al., Pitting corrosion of copper tubes for fire sprinkler system, Eng. Fail. Anal. (2022), 106631.
[10] M. Finšgar, et al., Polyethyleneimine as a corrosion inhibitor for ASTM 420 stainless steel in near-neutral saline media, Corrosion Sci. 51 (3) (2009) 525–533.
[11] A. Fateh, M. Aliofkhazraei, A. Rezvanian, Review of corrosive environments for copper and its corrosion inhibitors, Arab. J. Chem. 13 (1) (2020) 481–544.
[12] M. Finšgar, I. Milošev, Inhibition of copper corrosion by 1, 2, 3-benzotriazole: a review, Corrosion Sci. 52 (9) (2010) 2737–2749.
[13] O. Hollander, R.C. May, The chemistry of azole copper corrosion inhibitors in cooling waters, Corrosion 41 (1) (1985) 39–45.
[14] F.E.-T. Heakal, S. Haruyama, Impedance studies of the inhibitive effect of benzotriazole on the corrosion of copper in sodium chloride medium, Corrosion Sci. 20 (7) (1980) 887–898.
[15] F. Mansfeld, T. Smith, E. Parry, Benzotriazole as corrosion inhibitor for copper, corrosion 27 (7) (1971) 289–294.
[16] M. Finšgar, et al., A comparative electrochemical and quantum chemical calculation study of BTAH and BTAOH as copper corrosion inhibitors in near neutral chloride solution, Electrochim. Acta 53 (28) (2008) 8287–8297.
[17] Y.H. Lee, et al., Effect of benzotriazole on the localized corrosion of copper covered with carbonaceous residue, Materials 14 (11) (2021) 2722.
[18] E.A. Skrypnikova, S. Kaluzhina, I. Bocharova, Benzotriazole influence on copper pitting corrosion in hydrocarbonate-chloride solutions under different temperature, ECS Trans. 6 (24) (2008) 73.
[19] C. Yi, et al., Adsorption and protective behavior of BTAH on the initial atmospheric corrosion process of copper under thin film of chloride solutions, Sci. Rep. 8 (1) (2018) 1–15.
[20] S.H. Suh, et al., Pitting corrosion inhibition of sprinkler copper tubes via forming of Cu-BTA film on the inner surface of corrosion pits, Corrosion Science and Technology 18 (2) (2019) 39–48.
[21] S.H. Suh, et al., Inhibition of pitting corrosion failure of copper tubes in wet sprinkler systems, Corrosion Science and Technology 19 (2) (2020) 89–99.
[22] M. Tang, et al., Understanding copper pitting in drinking water pipes, Opflow 47 (8) (2021) 20–22.
[23] M. Sakai, A new type of silica-induced “moundless” pitting corrosion in copper observed in Japan, Heliyon 8 (8) (2022), e10110.
[24] D. Jones, Principle and Prevention of Corrosion. Second Ed. Environments vol. 334, Prentice Hall, New Jersey, 1992, pp. 214–217.
[25] G. Žerjav, I. Milošev, Protection of copper against corrosion in simulated urban rain by the combined action of benzotriazole, 2-mercaptobenzimidazole and stearic acid, Corrosion Sci. 98 (2015) 180–191.
[26] Y. Wu, et al., Effect of KI on improving copper corrosion inhibition efficiency of benzotriazole in sulfuric acid electrolytes, J. Electrochem. Soc. 140 (10) (1993) 2791.
[27] M. Musiani, et al., An electrochemical and SERS investigation of the influence of pH on the effectiveness of some corrosion inhibitors of copper, J. Electroanal. Chem. Interfacial Electrochem. 217 (1) (1987) 187–202.
[28] D.A. Lytle, M.R. Schock, Pitting corrosion of copper in waters with high pH and low alkalinity, J. Am. Water Works Assoc. 100 (3) (2008) 115–129.
[29] A. El Warraky, H. El Shayeb, E. Sherif, Pitting corrosion of copper in chloride solutions, Anti-corrosion Methods & Mater. 51 (1) (2004) 52–61.
[30] I. Suzuki, The prediction of pit initiation time for copper tubes in hot water from water composition, Corrosion Sci. 24 (5) (1984) 429–437.
[31] A. Stone, et al., The effects of short-term changes in water quality on copper and zinc corrosion rates, J. Am. Water Works Assoc. 79 (2) (1987) 75–82.
[32] Z. Chen, et al., Benzotriazole as a volatile corrosion inhibitor during the early stage of copper corrosion under adsorbed thin electrolyte layers, Corrosion Sci. 65 (2012) 214–222.
[33] D.A. Lytle, M.N. Nadagouda, A comprehensive investigation of copper pitting corrosion in a drinking water distribution system, Corrosion Sci. 52 (6) (2010) 1927–1938.
[34] M. Sosa, S. Patel, M. Edwards, Concentration cells and pitting corrosion of copper, Corrosion 55 (11) (1999).
[35] V. Lucey, Developments leading to the present understanding of the mechanism of pitting corrosion of copper, Br. Corrosion J. 7 (1) (1972) 36–41.
[36] J.H. Gross, Mass Spectrometry: a Textbook, Springer Science & Business Media, Heidelberg, 2004, p. 252.
[37] J.A. Whitby, et al., High spatial resolution time-of-flight secondary ion mass spectrometry for the masses: a novel orthogonal ToF FIB-SIMS instrument with in situ AFM, Adv. Mater. Sci. Eng. 2012 (2012).
[38] G.E. Lagos, C.A. Cuadrado, M.V. Letelier, Aging of copper pipes by drinking water, J. Am. Water Works Assoc. 93 (11) (2001) 94–103.
[39] Y.S. Kim, J.G. Kim, Electrochemical and quantum chemical studies of 1, 2, 3-benzotriazole as inhibitor for copper and steel in simulated tap water, Mater. Trans. 58 (1) (2017) 76–84.
[40] V. Brusic, et al., Copper corrosion with and without inhibitors, J. Electrochem. Soc. 138 (8) (1991) 2253.
[41] N. Khalil, Quantum chemical approach of corrosion inhibition, Electrochim. Acta 48 (18) (2003) 2635–2640.
[42] B. Markhali, et al., Electrochemical impedance spectroscopy and electrochemical noise measurements as tools to evaluate corrosion inhibition of azole compounds on stainless steel in acidic media, Corrosion Sci. 75 (2013) 269–279.
[43] A. Abdel-Gaber, et al., Inhibitive action of some plant extracts on the corrosion of steel in acidic media, Corrosion Sci. 48 (9) (2006) 2765–2779.
[44] I. Ahamad, R. Prasad, M. Quraishi, Thermodynamic, electrochemical and quantum chemical investigation of some Schiff bases as corrosion inhibitors for mild steel in hydrochloric acid solutions, Corrosion Sci. 52 (3) (2010) 933–942.
[45] K.H. Kim, et al., Effect of cobalt on the corrosion resistance of low alloy steel in sulfuric acid solution, Corrosion Sci. 53 (11) (2011) 3576–3587.
[46] M.S. Hong, et al., Effect of ascorbic acid on the pitting resistance of 316L stainless steel in synthetic tap water, Met. Mater. Int. 22 (4) (2016) 621–629.
[47] K. Aramaki, M. Hagiwara, H. Nishihara, The synergistic effect of anions and the ammonium cation on the inhibition of iron corrosion in acid solution, Corrosion Sci. 27 (5) (1987) 487–497.
[48] D. Tromans, R.h. Sun, Anodic polarization behavior of copper in aqueous chloride/benzotriazole solutions, J. Electrochem. Soc. 138 (11) (1991) 3235.
[49] S. Milić, M. Antonijević, Some aspects of copper corrosion in presence of benzotriazole and chloride ions, Corrosion Sci. 51 (1) (2009) 28–34.
[50] M. Scendo, J. Malyszko, The influence of benzotriazole and tolyltriazole on the copper electrodeposition on polycrystalline platinum from acidic chloride solutions, J. Electrochem. Soc. 147 (5) (2000) 1758.